A METHOD FOR HIGH RESOLUTION PEGDA HYDROGEL PHOTOPATTERNING AND HYDROGEL RELEASE IN MICROFLUIDIC DEVICES

by

Zhe Chen

A thesis submitted to Johns Hopkins University in conformity with the requirements for the degree of Master of Science in Engineering

Baltimore, Maryland

May 2021

© 2021 Zhe Chen

All Rights Reserved

Abstract

Soft microrobots are broadly applied in biomedical applications, including biosensing, diagnostics, drug delivery, and cell manipulation. There has been growing interest in automatic microfabrication of reliable and robust small scale hydrogels using the digital maskless photolithographic patterning method. In this thesis, we investigated the factors influencing photopatterning capability and efficiency in microfluidics, and we devised a method of releasing hydrogel patterns selectively for further applications. We applied benzophenone pretreatment of PDMS devices to form an oxygen quenching region surrounding the microfluidic channel to reduce the effect of oxygen inhibition. In addition, we made some optimizations to enhance the photopatterning efficiency in microfluidics, including adding a stopper to achieve stop-flow lithography, avoiding phase separation by introducing water soluble photoinitiator, and analyzing the effect of UV curing time on hydrogel sizes. In order to release the hydrogel patterns selectively, we utilized poly (acrylic acid) as the sacrificial layer, where its water solubility was controlled by Ca^{2+} ion and Na^{+} ion concentrations. We also designed a new method of assembling microfluidics by attaching two PDMS channels together and curing the sacrificial layer before device assembly for better lift-off specificity in microfluidics.

Advisor: Dr. Rebecca Schulman

Reader: Dr. Paulette Clancy

Acknowledgement

I am grateful to the generous help from many people during my research during the past two years. I would first like to thank the instruction from Dr. Rebecca Schulman and Mishe Rubanov for their insightful advice and inspiration throughout the projects. They also brought me many new angles and thoughts while looking into specific problems. I would also like to thank Joshua Cole, Heon Joon Lee, and all other lab members in the lab for their guidance and assistance on specific tasks. Their advice and comments helped me on improving current research experiments. Lastly, I want to thank my family and friends for their support and kindness. They showed great patience and gave me energy on working hard. Thank everyone for cooperation and commitment to the health and safety of our community during this hard time.

Table of Contents

List of Tables

List of Figures

Chapter 1

Introduction

1.1 Soft Microrobots

Robots are automatically operating machines controlled by programming that can accomplish a series of complex actions. Since the Industrial Revolution, modern mechanical robots have become increasingly appealing in engineering and service fields. For example, in the car manufacturing field, there are a variety of well developed robots that could complete specific repetitive missions such as spot welding, car assembly, painting, sealing, and coating.[1] Besides providing higher working efficiency with faster speed and higher consistency, robots can also achieve some challenging operations that could not be performed by humans according to machine designs and materials, including enduring extreme hazardous conditions and working without a break.

While some robots are designed in larger sizes to incorporate more elements in order to perform complicated functions, others are reaching much lower dimensions to be applied in very confined workspaces. Microrobots are one type of miniature automated robot that specifically range in size from 1 micrometer to 1 millimeter. With the features of robots in minuscular sizes, microrobots have been broadly applied in microscale biomedical applications, including biosensing,[2] diagnostics,[3] targeted drug delivery,[4] cell manipulation,[5] and other fundamental life sciences.[6] With less tissue damage than conventional clinical interventions, microrobotics studies are promising for future applications in the fields of biorobotics and therapeutic treatments.

Material choice of robot components is significant as it determines the physical properties and influences the functionality of automated machines. Rigid materials, such as metals and hard plastics, have been extensively used in conventional robot fabrications due to their physical strength and ease of casting. In comparison, soft robotics, the study of robots made from soft and elastic materials, has become an emerging field in recent years. Soft robots can accomplish safer and more robust functions in the interactions with humans or other biotic organisms because they have better compatibility and they can respond to more external stimuli, such as chemical concentration gradient, and they have higher degrees of freedom (DOFs) of motion.[7,8] With simpler and cheaper robotic components, soft robots could perform adaptive behavior using mechanical intelligence and simplify the controllers needed for physical interactions.[9] Furthermore, the flexibility of soft materials enables soft robots so that they can deform easily to adapt to unpredictable and sophisticated environments.[10]

As soft robots reach dimensions of microns, they are able to access smaller spaces, such as capillaries, to perform specific movements with higher precision. The interest in micropatterning of soft robots is growing with the new possibilities in biomedical applications. In order to assist robots in assessing and treating diseases in different organs within human body, Li et al. proposed a microrobot with an all-optic actuating and tracking system in the bloodstream.[11] For continuous and selective drug delivery to target cells, Park et al. developed a genetically modified bacteria-based microrobot with a combination of microsensor, microactuator and therapeutic agent.[12] In aspect of tissue engineering, Tasoglu et al, demonstrated a method of micro-robotic coding of three-dimensions soft materials for cell encapsulation.[13]

Different from the conventional robots that typically use electric, pneumatic, or hydraulic motors to actuate the versatile movements of the machine, soft microrobots generally use new

types of driving forces, including photothermal mechanisms,[11] chemomechanical,[12] and electromagnetic mechanisms,[13] for safe and robust actuations. These untethering signals are preferred for microscale applications as they could spread through a longer distance in very tiny and tortuous spaces in comparison to the traditional stimuli, which are the reasons why untethering signals would be more tempting to be used in soft microrobots for biomedical applications. In addition to safety and vitality, stimulus-specificity is also an important attribute in the researches of biomolecular actuations, because particular physiological responses would be expected at different locations or receptors in a complex, hierarchical structure or environment, such as a drug release system or a gene expression program.[14,15] Chemomechanical stimulation surpasses other untethering signals as its selective actuation could stimulate responses in specified areas. Also, the relatively straightforward synthesis and fast decomposition of chemicals also make it possible for accurate temporal control of microrobots. Specifically, Cangialosi et al. applied DNA sequences as actuators that could direct the shape change of micro-scale photopolymerized polyacrylamide hydrogels.[16]

Micropatterning enables rapid fabrications of soft microrobots with precise designed shapes. This is crucial for robots that would enter human bodies for specific biomedical applications. Based on Cangialosi et al.'s experiments, we expect to devise a method for the automatic implementation of photopatterning multi-domain DNA crosslinked hydrogels in microfluidics for soft microrobots. The objective of this project was to pattern small PEGDA hydrogels in specific shapes with resolutions in approximately 10 μm using UV exposure in a short time, and then release the hydrogel patterns selectively from the microfluidic channel.

1.2 PEGDA Hydrogel

One of the most distinct characteristics of soft microrobots is that they are constructed of soft materials. Among numerous types of soft matters, hydrogels exhibit prominent advantages in its safety, continuity, deformability and biocompatibility.[17] Hydrogels are three-dimension networks of hydrophilic crosslinked polymer chains.[18] Besides the swelling capacity of hydrogel due to its high stretchability and water containability, hydrogels can also display specific reactions to different external stimulations including temperature, pressure, pH, light, magnetism, molecular interactions and ionic strength.[19] As the greatest component in human tissues is water, the water absorbing ability and porous feature of hydrogels makes it an prevalent material for biomedical applications.[2]

Polyethylene glycol (PEG) hydrogels are one of the most prevalent biocompatible polymers.[20] PEG is a hydrophilic polymer or oligomer polymerized by ethylene oxide (C2H4O), with a repeating unit of -(CH2-CH2-O)-.[21] PEG is available in various structures including linear, star, branched and comb-like macromolecules.[20] Attaching to different reactive functional groups, PEG derivatives gain a variety of characteristics such as increased stability, water solubility and biocompatibility.[22]

Polyethylene (glycol) diacrylate (PEGDA) is a biologically inert hydrogel that polymerizes fast at room temperature with the presence of the photoinitiator and UV light. PEGDA is hydrophilic, elastic and can be tailored to include a variety of biological molecules such as DNA.[16] Therefore, PEGDA is an emerging scaffold material for tissue engineering and regeneration.[23] Figure 1 below shows the mechanism of crosslinking reaction to build a PEGDA network.

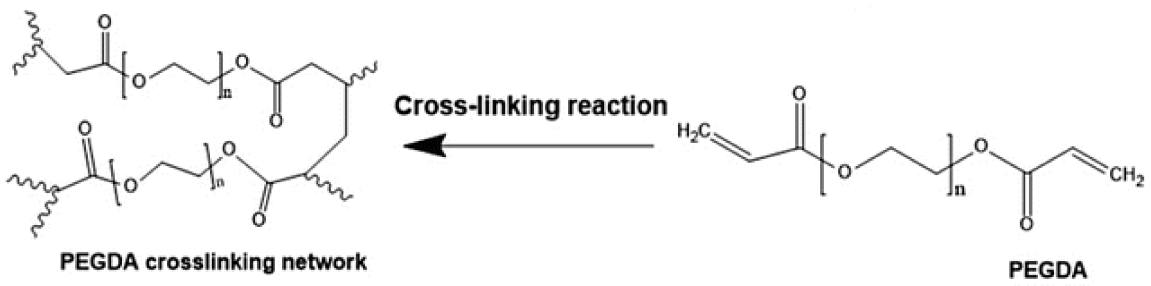

Figure 1.Polyethylene (glycol) diacrylate (PEGDA) crosslinking reaction.[24]

Free radical polymerization (FRP) is the most widely applied hydrogel crosslinking method for biomedical applications with the advantages of high reactivity, high conversion, and mild reaction conditions.[25] Thermal decomposition, photolysis, and redox reactions have been extensively used for the initiation phase. Specifically,we used photocrosslinking, or light-induced crosslinking, because of its exceptional ability for temporal and spatial control of the scaffold size and shape compared to other initiation systems.[26] Ultraviolet (UV) light at 365 nm was typically used to initiate the photopolymerization patterning process due to the high energy level containing within the electromagnetic irradiation.

1.3 Photopatterning and Microfluidic Devices

In order to obtain the desired hydrogel patterns in microfluidic devices via photocrosslinking, digital light processing (DLP) based stereolithography (SLA) was applied. Introduced by Texas Instrument in 1993, DLP uses a digital micromirror device (DMD), with millions of micromirrors being controlled by binary signals, to reflect the UV light emitted from UV LED and project the computer-aided design (CAD) patterns directly on the substrates to achieve digital maskless photolithography.[27,28] Because DLP cures the entire layer at once, it cures the patterns faster and therefore is more efficient compared to other stereolithography techniques.[29]

For lower polymerization scale and better observation, the patterns were formed with a 20X Nuv patterning lens on a microscope. The microscope setup is shown in Figure 2.[30]

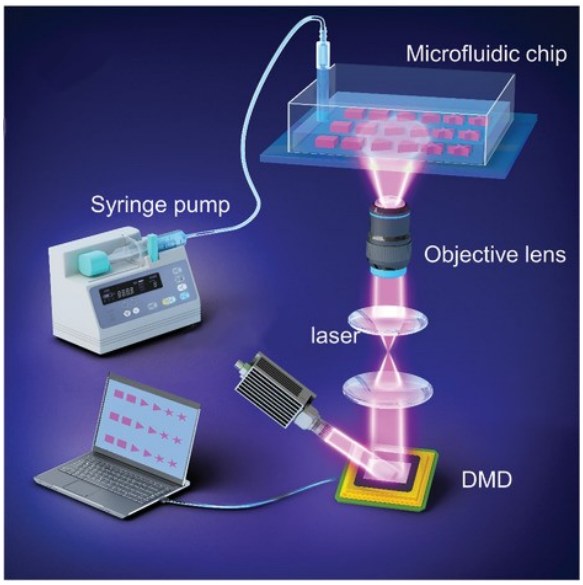

Figure 2. Microscope setup for photopolymerization of hydrogel in microfluidic chips via DMD.[30]

With the purpose of accomplishing automated multi-domain DNA hydrogel photopolymerization, a microfluidic device is an optimal substrate for containing the pre-polymerization solutions and proceeding patterning process. With inlets and outlets, the microfluidics are available for multiple flows and low dead volumes.[31] Besides, automatic control of the photopatterning process could be achieved as the switches and pumps could be controlled by programming.[32]

Compared to conventional materials, polydimethylsiloxane (PDMS) has been one of the most appealing materials for microfluidics with several advantages. PDMS could tolerate higher pressure in the channel before leaking due to its excellent deformability.[33] The UV transparency of PDMS is also a necessary property for UV photopolymerization to generate hydrogel patterns.[34] PDMS is very easy to mold as the base elastomer and curing agent are both in liquid phase at room temperature, and the curing temperature for PDMS to be fully cured is 80 ºC for 2 hours.[35] Besides, the good gas permeability of PDMS makes it possible for residual air bubbles to escape from PDMS under high liquid pressure.[36] PDMS is also a cost-effective material because of its relatively low price.[37] We fabricated the microfluidic channel by compiling the glass slide to a PDMS channel groove which had been modulated by SU-8 on silicon wafer and hole punched, and then

annealing by oxygen plasma. The schematic is shown in Figure 3 and the detailed microfabrication method was stated in the method section.

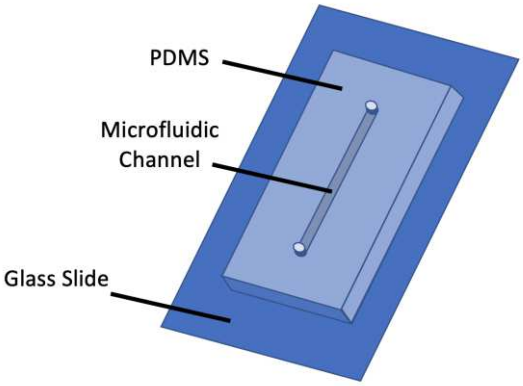

Figure 3. Schematic of PDMS glass microfluidic device.

In microfluidic channels, the flowrate of solution becomes a significant factor for the synthesis of polymeric particles. Early polymerization works were usually done on continuous flow lithography (CFL), with the polymerization process performed in a constant laminar flow microfluidic system.[38] Although the solidified polymers could be formed instantly and flushed out of the channel with flow in CFL, it is hard for synthesizing polymer particles in complex structures. Dendukuri et al. proposed stop flow lithography (SFL) in PDMS microfluidic chips for better hydrogel resolutions and complicated pattern shapes.[39] Because smaller pattern sizes were expected, we applied SFL techniques in our experiments that performed the polymerization in a stationary phase before washing out of the microfluidic channels.

1.4 Challenges and Goals

The goals of this thesis were to: a) Photopattern hydrogel quickly with resolution of approximately 10 μm in microfluidics by i) reducing oxygen inhibition, ii) using stop-flow lithography, iii) solving phase separation in microfluidics, iv) and choosing specific UV exposure time. b) Release the hydrogel patterns selectively in microfluidics by coating the channel with a sacrificial layer and adjusting its water solubility by addition of specific chemicals.

1.4.1 Oxygen inhibition

We were expecting to pattern hydrogels with small scales to 10 micrometers to mimic the size of yeast cells in microfluidics, because DNA could diffuse faster in smaller hydrogels, and thus respond to the outside actuations in a shorter time. However, oxygen inhibition became an obstacle in patterning PEGDA hydrogels with small resolutions as the PDMS microfluidic device is very permeable to oxygen.[40] Oxygen inhibition is useful sometimes for non-attachment of hydrogel patterns on microfluidic channel walls,[39] but it could be a potential problem when oxygen act as a comonomer in free-radical polymerization to generate side products and hinder the curing rate via the reactions shown in Table 1.

No.	Reaction	Stage
1	$[PI]^T + O_2 \rightarrow PI$	Initiation
2	$R\bullet + O_2 \rightarrow R\text{-}O\text{-}O\bullet$	Propagation
3	$R\text{-}M\bullet + O_2 \rightarrow R\text{-}O\text{-}O\bullet$	Propagation
4	$R\text{-}O\text{-}O\bullet + R\bullet \rightarrow R\text{-}O\text{-}O\text{-}R$	Termination

Table 1. Reactions of oxygen inhibition on free-radical polymerizations.

Oxygen inhibition could restrain the free-radical polymerization in several different aspects: oxygen could quench photoinitiator (PI) at excited state (Reaction 1), and oxygen could react with initiating and propagating radicals to form peroxyl radicals which are not energetically favorable towards polymer propagation(Reaction 2, 3), where the peroxyl radicals are more likely to proceed radical-radical combination to terminate the polymerization (Reaction 4).[41] Hence, the existence

of oxygen in polymerization process could defer polymerization rates, increase induction phase, reduce conversion ratio, shorten the polymer kinetic chain length, and create tacky surfaces.[42]

There have been numerous directions towards overcoming the oxygen inhibition or reducing its influences, including blocking oxygen from diffusing into microfluidic channels, decreasing oxygen solubility of fluid in the channel, and accelerating the polymerization rate. First, approaches were devised for blocking oxygen outside of the entire polymerization system. Closed systems were designed for the encapsulation of microfluidic chips, and inert gases, such as nitrogen (N_2), helium (H_2), and carbon dioxide (CO_2), were used to exclude oxygen inside the system.[43] Physical barriers, including liquid and wax barriers, were also applied to prevent oxygen from diffusing through PDMS and reach polymer precursor solution.[44] Besides, reducing oxygen solubility in pregel solution is another direction to decrease the side effects brought by oxygen during photopolymerization. oxygen scavenger, like sugar, could be added in the pregel solution so that the oxygen concentration could be lowered inside the microfluidic channel.[45]

1.4.2 Release hydrogel patterns from microfluidic channel

In order to better actuate the PEGDA hydrogels to complete several actions such as bending, twisting, swelling, and shrinking directed by different DNA sequences, we wanted to be able to lift the hydrogels off from the glass slide in the microfluidic channel and collect them at the microfluidic channel's outlet after the structures are patterned.[16] With the goal of patterning multi-domain DNA crosslinked hydrogels automatically, the approach to liftoff that we take should allow multiple solutions to flow through the microfluidic channel during multiple patterning stages for different types of domains, and allow previously formed hydrogel patterns to remain anchored to the channel walls until all patterning stages are complete. We expected to photopattern several

hydrogels using pregel solutions containing different DNA strands, and release all the patterns at once, so the lift-off selectivity of hydrogel patterns becomes significant. Sacrificial layers are considered to be an optimal approach to detach the hydrogels from the channel at selective time points as they are typically used in photolithography for surface microfabrication and etching of polycrystalline silicon.[46] As hydrogels are mostly composed of water, they are highly hydrophilic so that hydrogels are easily sticked to the glass slide in the microfluidic channel.

There are some other factors affecting the photopatterning efficiency inside the microfluidic channels, including the flow rate of pregel solution, photoinitiator choices, and UV light exposure time. We tried to use stop-flow lithography for hydrogel photopatterning in microfluidics for better patterning resolutions, but the flow did not stop for more than minutes after the pumping had been stopped. There was a pressure drop between the PDMS microfluidic channel and the ambient environment because the PDMS could be deformed due to pumping pressure in microfluidics as shown in Figure 4. Also, this pressure difference was difficult to balance in a short time when the channel because of the hydraulic resistance of the capillary tubing.[47] We utilized a syringe connecting to the outlet tubing as a microfluidic flow stopper so that the flow in the channel would stop almost instantly.

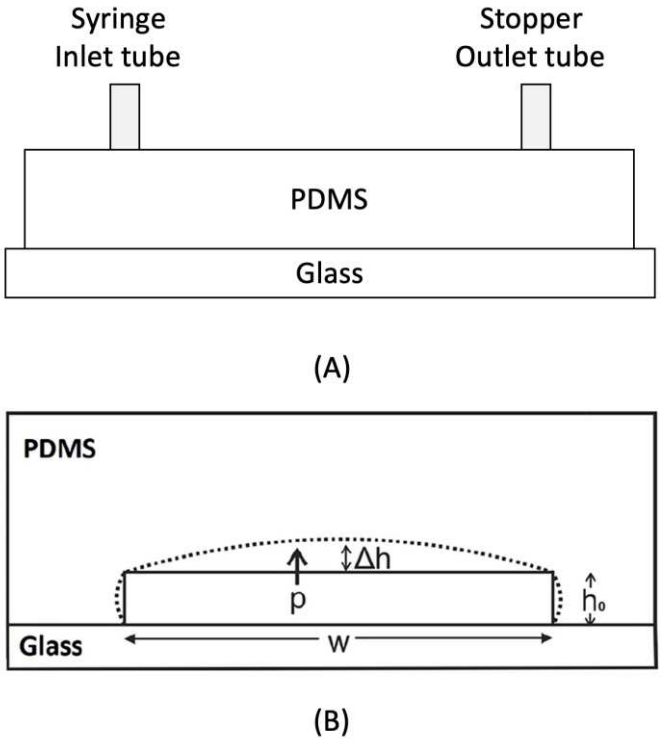

Figure 4. Schematic of (A) microfluidic device setup for fast stop-flow lithography and (B) pressure influence on PDMS deformation.

Phase separation became a problem in microfluidics as the photoinitiator we chose in previous experiments were Omnirad 2100 which is hydrophobic. The photoinitiator continued precipitating out of the pregel solution after mixing, resulting in a various photoinitiator concentration of the pregel solution and therefore an inconsistency in patterning ability. Besides, the Omnirad phase would accumulate inside the microfluidic channel as it sticked to the PDMS walls easily, which would sabotage the following crosslinking process if multi-domain photopatterning is conducted. To avoid overexposure, controlling UV exposure time is one crucial factor during photopolymerization. Overexposure of UV light during the hydrogel formation step could result in greater extent of PEGDA crosslinking and further influence the hydrogel mesh size.[48]

In this work, we applied benzophenone (BP) to form an oxygen quenching region in PDMS to block oxygen from diffusing into pregrel solution. We also utilized polyacrylic acid (PAA) to form a sacrificial layer to control the selective release of hydrogel patterns from the microfluidic channel. Furthermore, we tried a few approaches to achieve a higher photopatterning efficiency in microfluidic channels, including balancing the channel pressure, trying water-soluble photoinitiator, and measuring pattern sizes under different UV exposure time.

Chapter 2

Results and Discussion

2.1 Photopatterning smaller PEGDA hydrogels and reducing oxygen inhibition

One of our goals is to obtain small patterns with low feature sizes below 20 μm in a microfluidic channel at a height of 20 μm. We initially tried photo-patterning directly with the protocol adapted from Dorsey et al. DNA hydrogel photocrosslinking method.[49] Although large circle patterns with diameters of around 40 μm could be generated in 100 μm high microfluidic channels, oxygen inhibition became a significant problem when the method was applied to pattern the same shaped structures in the channel with the height of 20 μm. As stated in the introduction, oxygen inhibition could hinder the photopolymerization process, making it difficult to pattern small hydrogels, and potentially deforming the patterned shapes when hydrogel patterns do form, as shown in Figure 5.

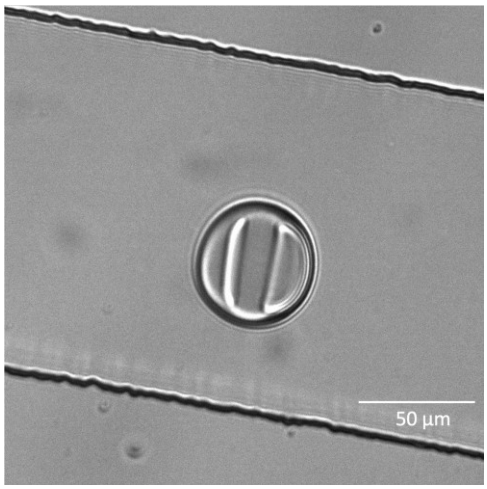

Figure 5. Oxygen inhibition deformaed the shape of a hydrogel patterned with a 60 µm diameter mask in a 20 µm height microfluidic device.

In order to reduce the effects of oxygen inhibition while only making minimal changes to our original hydrogel photopatterning protocol in microfluidics, we introduced 10 % w/v benzophenone dissolved in ethanol to treat the PDMS glass device for around 30 minutes prior to the addition of pregel solution.[50] Benzophenone ($(C_6H_5)_2CO$) and its derivatives are typically used as UV curing agents, fragrance enhancers, and UV blockers in a variety of cosmetic products.[51] It has been shown that molecular oxygen would be depleted during its interactions with sufficient benzophenone via quenching, photobleaching, and terminating processes.[52] Therefore, in this method, we applied benzophenone as an oxygen scavenger diffusing through the inner surface of the PDMS elastomer, forming an oxygen quenching region on the PDMS side. This benzophenone matrix in PDMS then blocked the oxygen from arriving at the photopolymerization area in the microfluidic channel.

We tried photopolymerization of PEGDA 575 with 50, 45, 40, 35, 30, 25, and 20 µm diameter circular masks with and without benzophenone treatment separately in a 20 µm high microfluidic channel using Omnirad 2100 as the photoinitiator. With the benzophenone treatment,

we managed to obtain PEGDA 575 hydrogel circles at around 10 µm in diameter. We tried patterning hydrogel circles using the same mask size with a diameter of 30 µm in separate microfluidic channels with different pretreatments. We were only able to obtain a circle hydrogel in the channel pretreated with benzophenone modification, and there was no indication of any pattern formation in the untreated channel, shown in Figure 6.

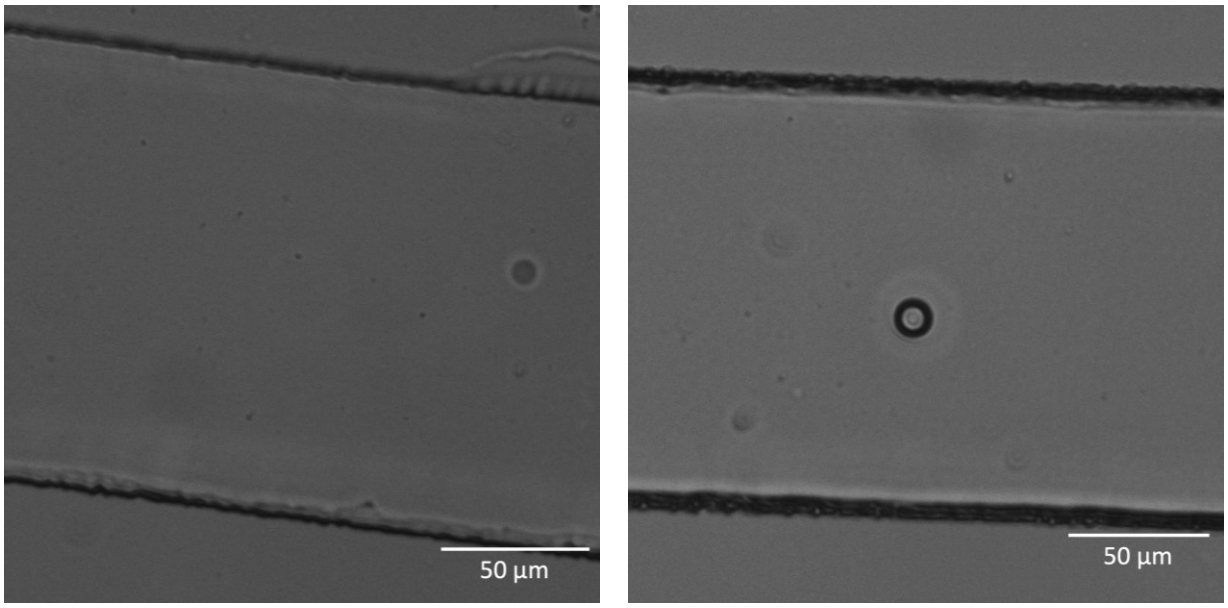

A B

Figure 6. Photopatterning in 20 µm height channels without and with benzophenone pretreatment, 5 seconds UV exposure using a circular mask with the diameter of 30 µm was applied. A: Without benzophenone pretreatment, no pattern was formed. B: With benzophenone treatment, a pattern was formed.

The result shown in Figure 6.B indicated that the benzophenone pretreatment of microfluidic channels helped improve the photopatterning ability of PEGDA hydrogels. As shown in Figure 7, benzophenone diffused through the PDMS elastomer and formed a layer encapsulating the PDMS microfluidic channel. Usually molecular oxygen hinders the photopolymerization

initiated by benzophenone by inhibiting the hydrogen abstraction, but benzophenone can also act as an oxygen scavenger when present at sufficiently high concentrations.[52] Therefore, the benzophenone layer surrounding the microfluidic channel was applied as an oxygen quenching region that exhausted all oxygen existing in PDMS, and thus the oxygen concentration in microfluidic channel remained at a relatively low level.

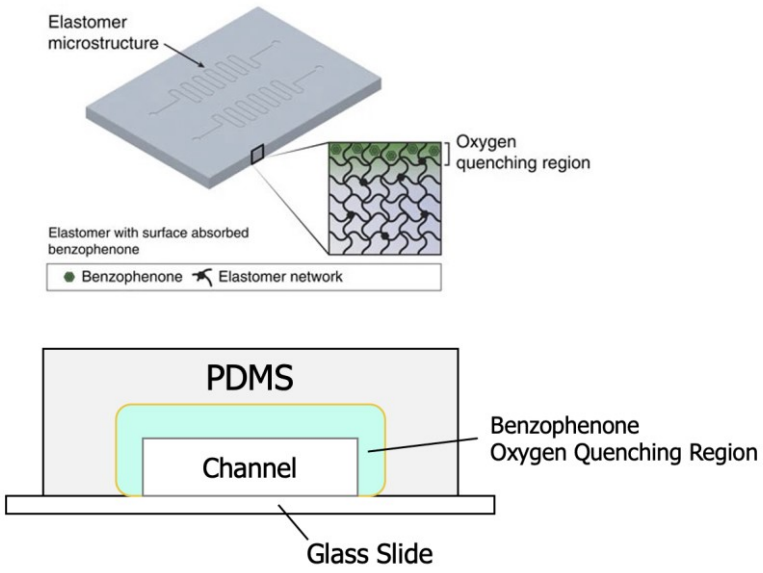

Figure 7. Oxygen quenching region in the PDMS elastomer formed by diffusion of benzophenone.[50]

In addition, a small amount of benzophenone could diffuse back from PDMS to the pregel solution and contribute as a UV curing agent to enhance the photopolymerization process. Excess pregel solution flowed through the microfluidic channel to expel the benzophenone solution before the process of UV photocuring the PEGDA hydrogel. The benzophenone concentration in PDMS became higher than in the microfluidic channel after the addition of pregel solution, and some benzophenone diffused backward from the PDMS to the pregel solution due to the concentration gradient. Hence, the benzophenone diffused back to the microfluidic channel could possibly assist the photopolymerization process.[53]

We applied 10% w/v benzophenone in ethanol to pretreat the PDMS microfluidic channels for 30 minutes for a sufficient diffusion to ensure there would be enough benzophenone in PDMS reacting with molecular oxygen during the photopatterning process. Ethanol was utilized as the solvent to dissolve benzophenone and assist the diffusing process of benzophenone, and it could be substituted by other organic solvent such as acetone. According to the experiments performed by Schneider et al, 10% w/v benzophenone dissolved in acetone could have an adequate diffusion to the PDMS in around 10 minutes as shown in Figure 8, and further diffusion were expected to be relatively slow and time consuming.[52] In comparison, continuous flow of 10% w/v benzophenone in acetone for 10 minutes could be a better pretreatment strategy for generating the oxygen quenching region in PDMS.

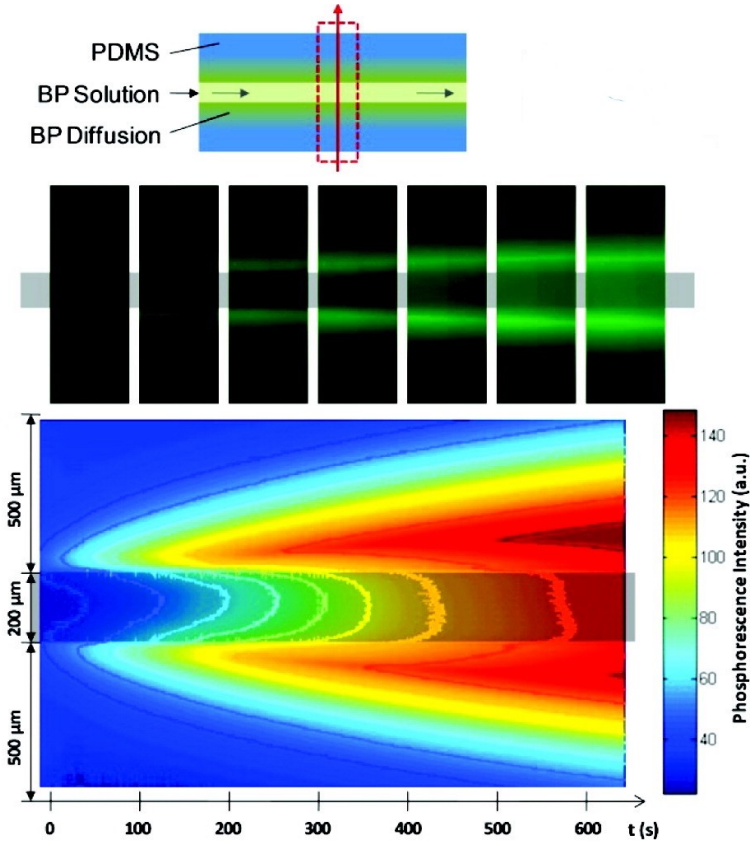

Figure 8. The diffusion profile of 10% w/v benzophenone in acetone through a 200 µm wide and 100 µm deep PDMS channel with time. Photoluminescence intensity was applied to indicate the diffusion of benzophenone.

There are many other strategies that could be used to reduce the influence of oxygen inhibition and further increase the photopatterning ability in microfluidic chips, as discussed in the introduction. Compared to the conventional methods, such as building a closed outer system for the microfluidic device, or reducing the oxygen solubility in the pregel solution by adding specific oxygen scavengers or adjusting the environmental temperature, benzophenone pretreatment was relatively simple and straightforward to apply in any microfluidic channel without a drastic change in the recipe of hydrogel precursor solutions, which minimizes the potential effects on the photopatterning procedure.

As we patterned hydrogels with different mask sizes, we found that the actual pattern sizes were not exactly matched to the mask sizes we were using. The potential reasons could be an unstable photoinitiator concentration in pregel solution, wrinkles during the PDMS microfabrication from the silicon molds, or UV light scattering through the glass slides. We drew a calibration curve Figure 9 for the actual pattern sizes versus the mask sizes. The result showed that actual pattern circles were generally smaller than the mask circles, and there was a linear trend for the trial with benzophenone treatment, where the calibration equation was $y = 1.5067x - 29.441$ with the R^2 value of 0.9901.

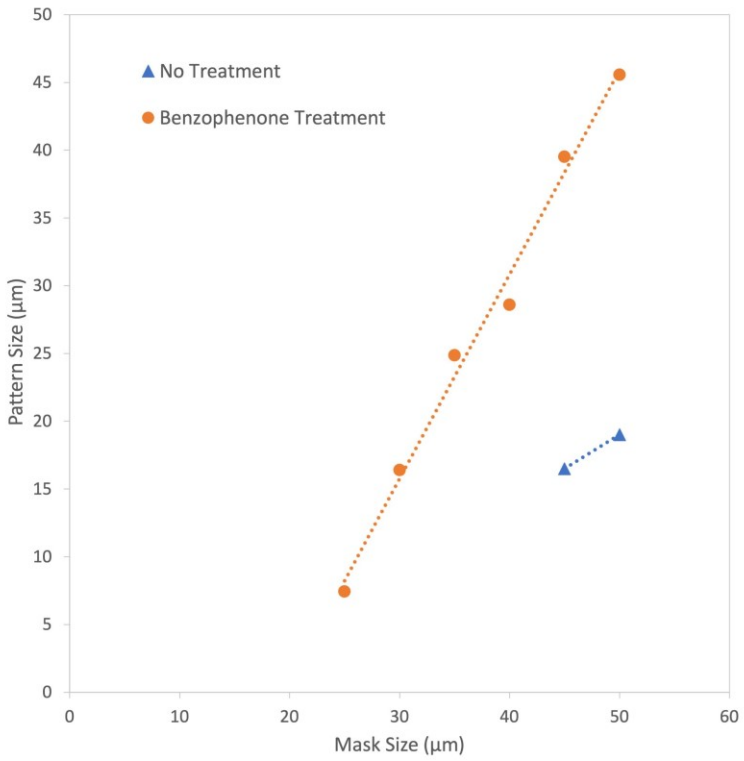

Figure 9. Actual pattern sizes versus mask sizes with different treatment.

The linear trend shown in Figure 9 indicates that the patterning ability was relatively stable in the microfluidic channel, and we can use this trend line to predict the general pattern sizes obtained in a different microfluidic channel with the same experimental settings. However, because the actual hydrogel pattern sizes are very sensitive to the setup changes, the curve needs to be recalibrated after changes in microscope stages or light focuses.

Furthermore, after the photocrosslinking process, we often found the appearance of light scattering, resulting in a deep circle inside and a shallow circle outside, as shown in Figure 10. For our apparatus, the focus plane of the digital mask did not match exactly to the focus of the microfluidic channel with a few microns difference in height. When we focused the microscope objective to the channel during the photopatterning process, the light scattering of the mask appeared shown as the blue LED indicator image in Figure 10.

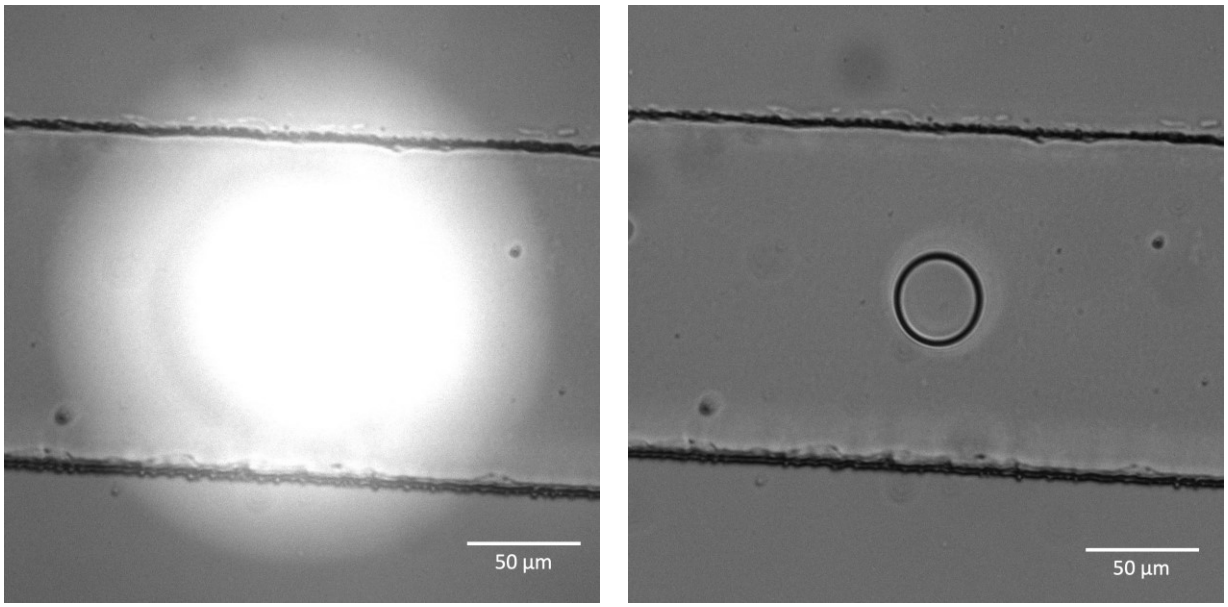

Circle blue LED Pattern Result

Figure 10. Light scattering of the 50 µm circular digital mask when the microscope objective was focused on the microfluidic channel and the resulting pattern.

The figures showed that the UV exposed region was larger than the size of the actual circle, indicating that the light intensity at the center was strong enough to cure hydrogel crosslinking in a short time. Although the light intensity at the outer region was not strong enough, it partially polymerized the hydrogel and formed a relatively blurry circle surrounding the small circle. This phenomenon became more apparent when the light was more scattered. In order to better align the microfluidic channel and focal plane of the digital masks, it could be a feasible and straightforward approach to install a z-stage to the microscope platform.

Also, we plotted the ratio of actual patterns to the masks versus the mask sizes, shown in Figure 11. It was revealed that the ratio decreased faster as mask sizes got smaller, which could be an indication that the influences of light scattering became an increasingly significant factor for

smaller patterns, which also partially explained why it was harder to pattern hydrogels in the resolutions below 10 µm.

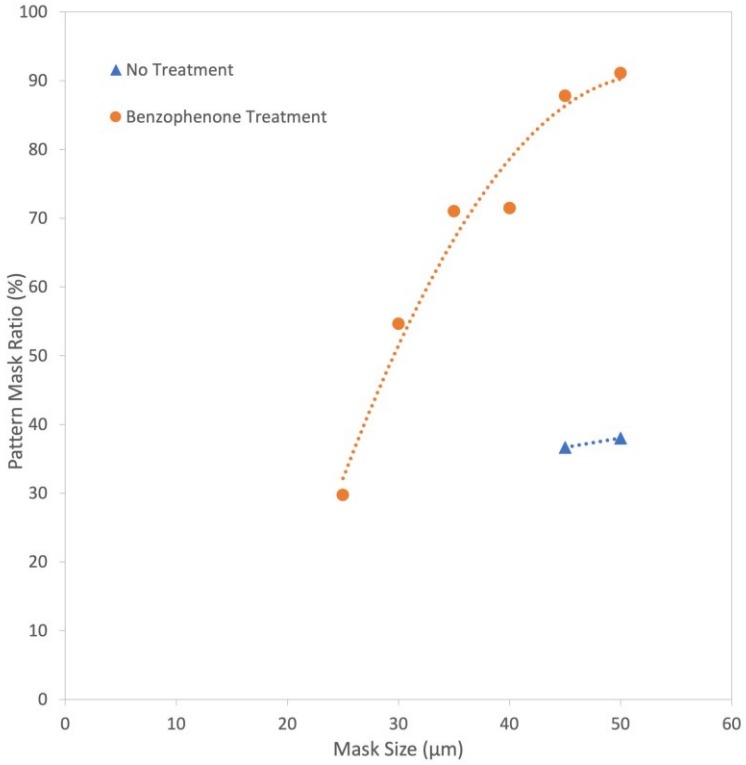

Figure 11. Pattern mask ratio versus mask sizes with different treatment.

2.2 Optimizations of a Photopatterning Protocol to Improve Photopatterning Capability and Stability

During the process of PEGDA hydrogel photopolymerization in 20µm height microfluidic channels, we found several factors, such as the flow inside the channel and phase separation, that could affect the capability and stability of pattern formation. In order to develop a fast and reliable method of photopatterning stable microscale hydrogels, we came up with some optimizations before and during the photopolymerization process, including adding a stopper on the channel

outlet of achieve stop-flow lithography quickly and switching the photoinitiator to solve phase separation problem in microfluidics.

Inlet tube and outlet tube connecting to the microfluidic channels make it easy for automated multi-flow photopolymerization process and waste collection in microfluidic devices. We could simply switch syringes that connected to the inlet tube to change solutions, and the waste could be collected in a large container that connected to the outlet tube. Despite the convenience of photopatterning automation, it became difficult for the flow to stop inside the microfluidic channel after the syringe had stopped pumping when the inlet and outlet tubes were connected. This is because the PDMS is very deformable, and the microfluidic channel will expand as the pressure is applied to the PDMS walls. When solutions flowed through the microfluidics, high pressure was applied by a syringe pump to push the solution through the channel, which resulted in PDMS channel deformation at the same time. After we stopped pumping, the pressure in the microfluidic channel remained high because of PDMS deformation and the flow continued in the channel until the PDMS turned back to the original shape and the pressure inside and outside the microfluidics became balanced. When microfluidics were connected to the tubes, it would take longer time for the flow to stop because of hydraulic resistance of the capillary tubing. The continuous flow in microfluidics during the photopolymerization process could result in pattern deformation, sabotage to pattern resolution, or even incapability of hydrogel generation. This situation would be amplified in a smaller microfluidic channel and thus the solution requires a much longer waiting time to stop in the channel, which is not desirable for the stop-flow lithography we are using. In order to stop the flow inside the microfluidic channel in a short time, we introduced a syringe as a microfluidic flow stopper connected to the tube at the outlet. Flows

were stopped instantly and patterns were reliably obtained with this method, as shown in Figure 12.

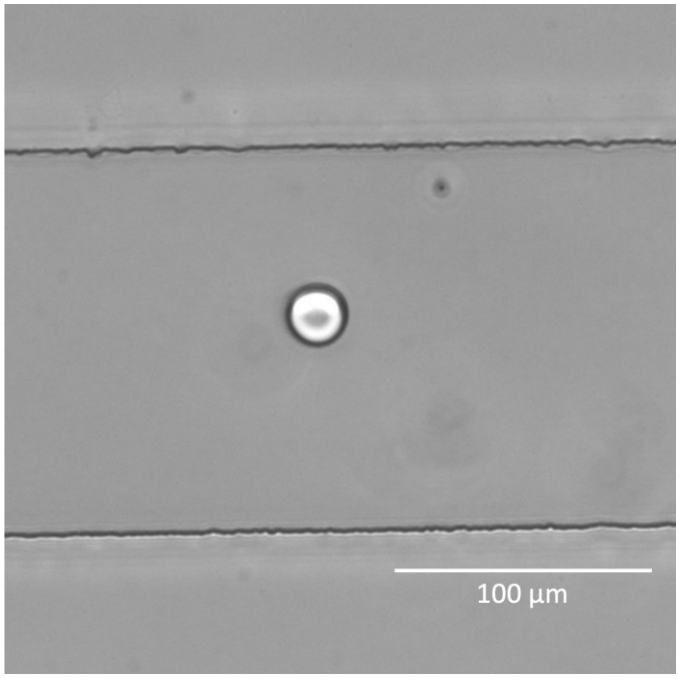

Figure 12. Pattern formed with 50 µm mask and 5 seconds UV exposure in a 20 µm microfluidic channel with stop-flow lithography.

The microfluidic devices we are using are assembled by the PDMS and the glass slide via oxygen plasma treatment, where the PDMS is hydrophobic and the glass is more hydrophilic. The hydrophobicity of the photoinitiator we used (Omnirad 2100) was high and it adhered to the PDMS channel walls during and after the photopatterning process. The photoinitiator could occupy part of the channel, which would probably result in phase separation, shown in Figure 13, and therefore alter the patterning ability inside the channel because the component concentration of the hydrophobic phase in pregel solution was primarily photoinitiator. We could only obtain a large blurry pattern or even no pattern in the hydrophobic phase, shown in Figure 14. Also, Omnirad 2100 continually precipitated out from the moment the pregel solution was prepared. This condition fluctuates the patterning stability, where the calibration line of actual pattern size versus

mask size could be different with different waiting times after vortex mixing. Also, the hydrophobic phase would grow inside the microfluidic channel because of the precipitation of the photoinitiator, and could probably take up the entire channel in the end. This phenomena could be severe especially in smaller 20 µm channels because of the higher surface to volume ratio.

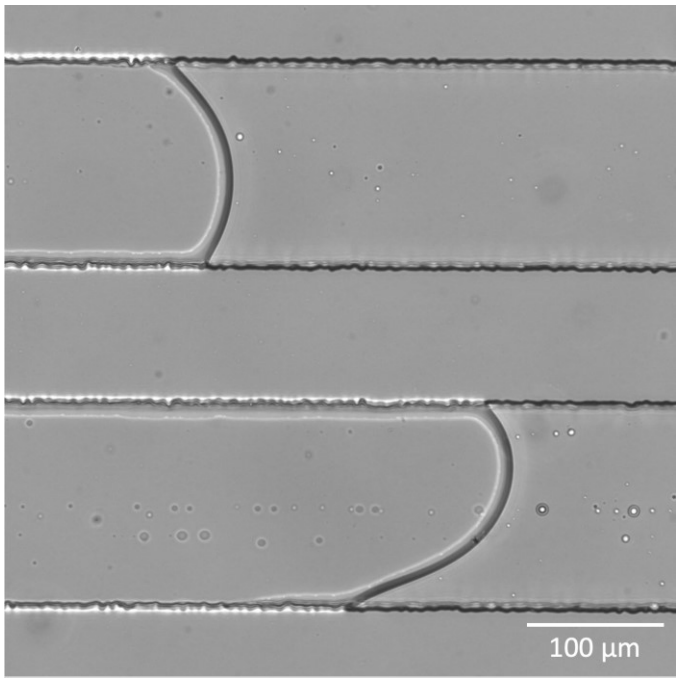

Figure 13. Phase separation in 20 µm microfluidic channel.

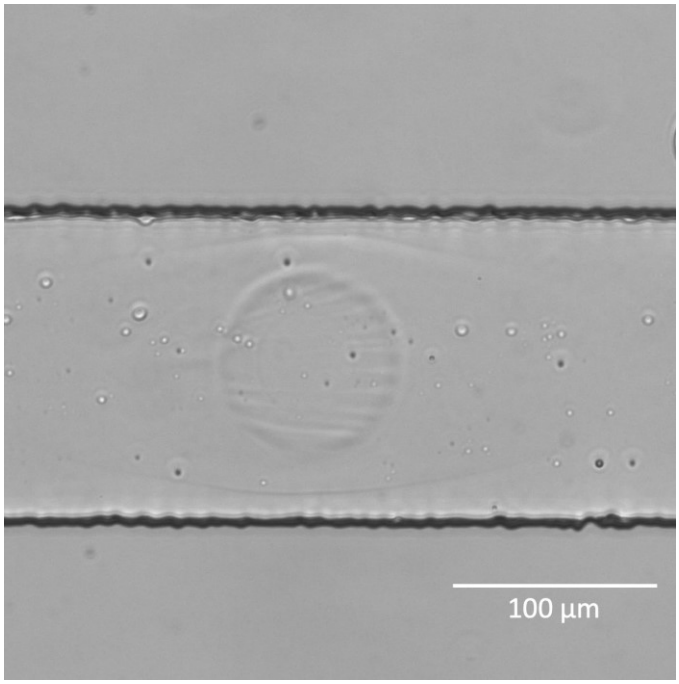

Figure 14. Patterning attempt in hydrophobic phase in 20 µm microfluidic channel. Large and opaque circle pattern formed with 50 µm mask, with a superficial ellipse outside the circle.

In the process of photopatterning, we found that waiting a longer time for the settling of pregel solution then taking only the supernatant of solution could mitigate the phase separation problem in microfluidic channel. However, the waiting time could not be too long because photopolymerization of PEGDA 575 began from the moment the pregel solution was mixed as we could not completely avoid light from the ambient environment. We tried centrifuging the mixture for 30 seconds after vortex mixing the pregel solution to accelerate the photoinitiator precipitation process. In this situation, the phase separation was mitigated and we were able to form patterns using a shorter exposure time. The pattern formed with centrifuging was shown in Figure 15.

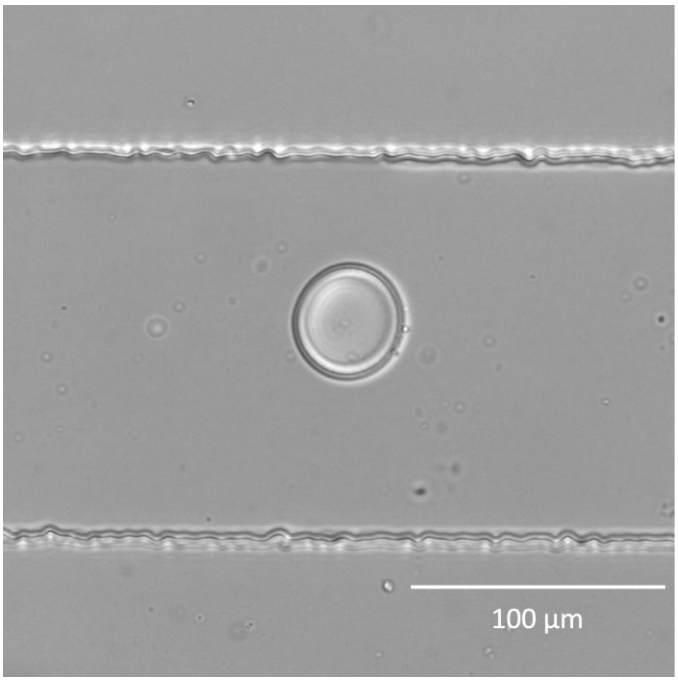

Figure 15. Pattern formed with a 50 µm mask in a 20 µm microfluidic channel after the pregel solution was centrifuged.

Although we could get a more stable pattern in smaller channels by centrifuging the pregel solution to speed up the precipitating process of Omnirad 2100, the hydrophobic photoinitiator was hard to rinse from the channel using flowing water and 1XTAE solutions. The resulting accumulation of Omnirad 2100 could affect the cleanness of microfluidic channels where multi-flow or multi-domain patterning would occur. For more stable patterns and better cleanness in microfluidic channels, we introduced a new photoinitiator, lithium phenyl-2,4,6-trimethylbenzoylphosphinate (LAP). Compared to Omnirad 2100, LAP has better cytocompatibility, and the concentration of LAP photoinitiator required for photopolymerization is much lower than that of Omnirad 2100.[54] As opposed to Omnirad 2100, LAP is a hydrophilic photoinitiator, and therefore it will not cause any phase separation. With LAP as a photoinitiator, we observed a higher photopolymerization efficiency with a lower photoinitiator concentration. In the previous pregel solution protocols, we used 3% Omnirad 2100, but now only 0.1% w/v LAP

is enough to obtain circle patterns in microfluidic channels. Although the curves with different photoinitiators are different, according to the calibration lines shown in Figure 16, the protocol with LAP as a photoinitiator showed a better patterning ability and a more uniformed phase after several flows.

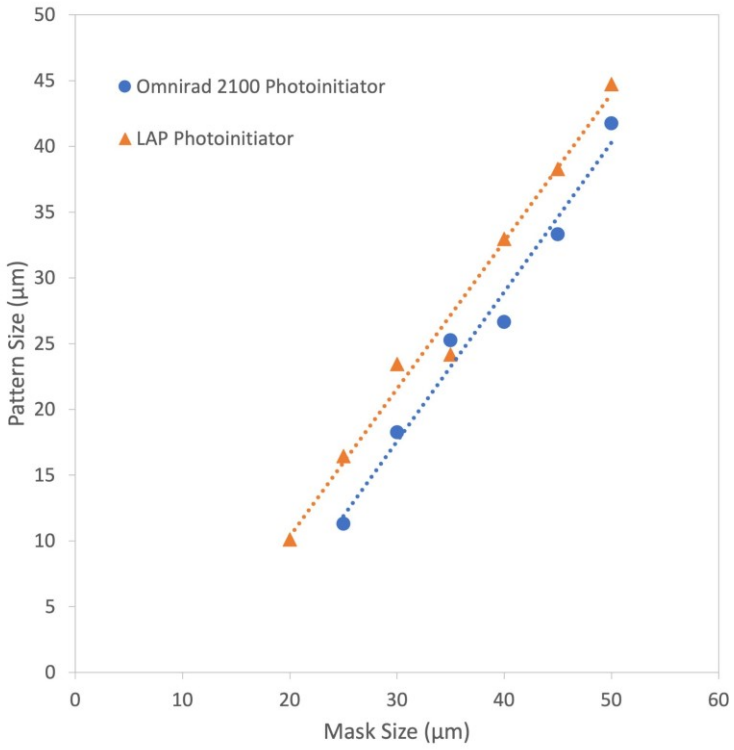

Figure 16. Calibration lines of actual patterns versus mask sizes with different photoinitiator.

Exposure time is also a factor that could have an effect on the actual pattern sizes. To investigate the influence of UV exposure time, we tried the same mask sizes with different photopatterning times. We conducted the experiment in 20 µm microfluidic channels with the same masks at 5, 4, 3, 2, and 1 seconds of UV exposure separately, shown in Figure 17. Three trials were used for each point to generate the plot. From the result we observed a slight shrink of pattern sizes with shorter UV exposure time, but overall the influence of UV exposure time did not result in a significant influence on patterning ability and actual pattern sizes. The effect of UV exposure time is reduced as mask sizes decrease according to the plot.

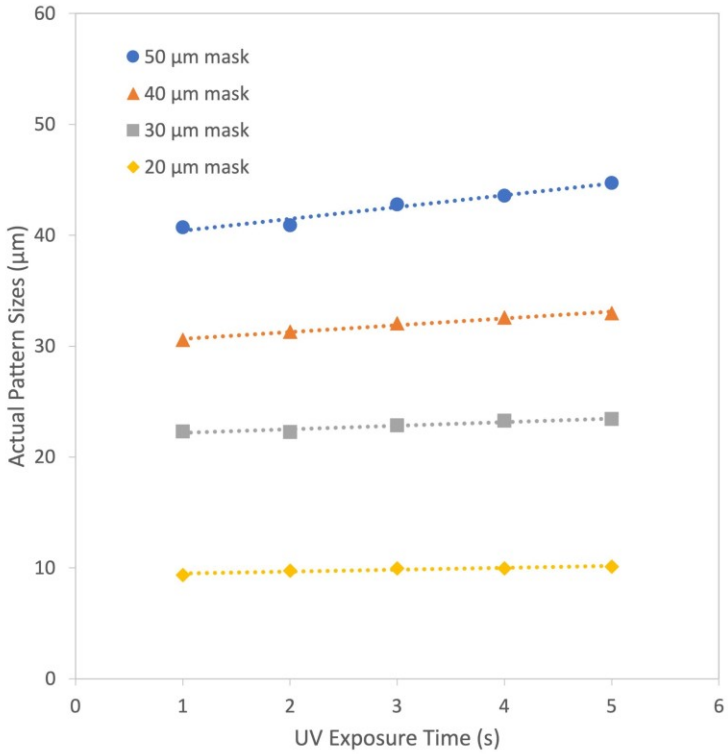

Figure 17. Actual pattern sizes versus UV exposure time with different mask sizes.

2.3 Release Hydrogel Patterns from the Microfluidic Channel with Sacrificial Layer

The function of movement is one basic characteristic of soft microrobots, and floating hydrogel patterns are required for many biomedical applications such as drug delivery. In order to better actuate the PEGDA hydrogel to complete various actions such as moving, bending, twisting, swelling, and shrinking as directed by diverse DNA sequence systems, it is desired to lift the patterns off from the microfluidic channel and collect them at the outlet.

As our 20 μm microfluidic devices are assembled by attaching the PDMS to a flat glass slide through oxygen plasma treatment, the channel is composed of two different materials, where

the PDMS is relatively hydrophobic and the glass is more hydrophilic. Therefore, we expected that hydrogel patterns would be stickier to the glass part due to the high water content of hydrogels. Then we designed an experiment that pushed the water hard by hand through the channel to observe whether the pattern would stay in the channel and which side would move first, which is shown in figure 18 below.

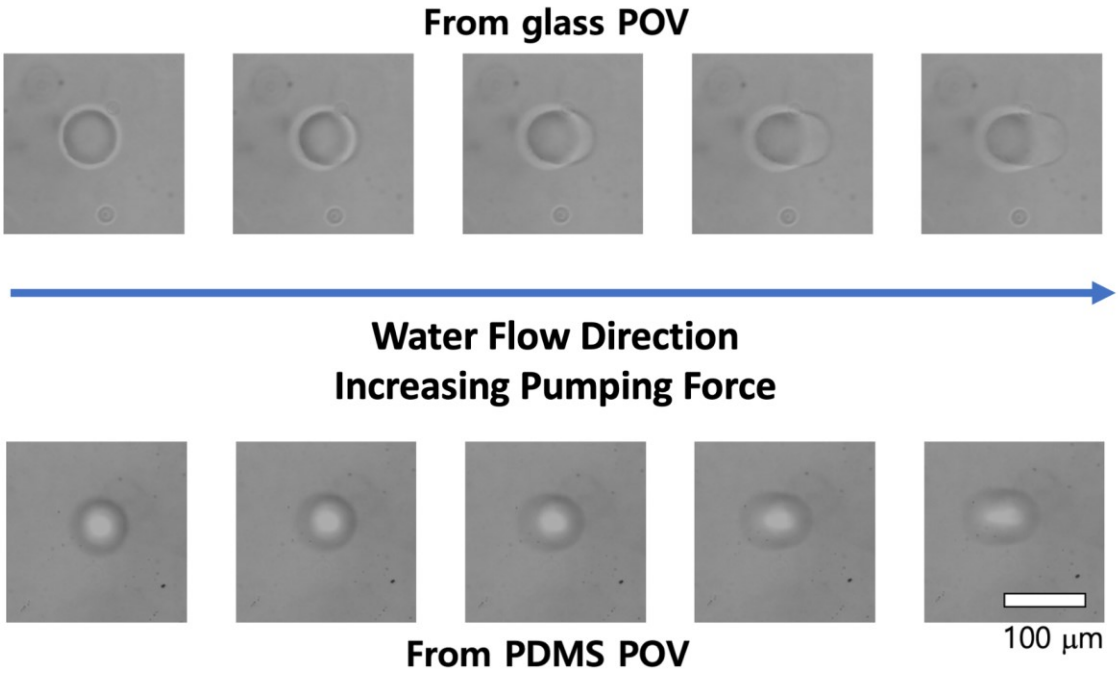

Figure 18. Hydrogel pattern deformation when water was through the microfluidic channel. Water flowed from left to right and pumping force increased from left to right.

The images taken from both glass point of view and PDMS point of view show that the hydrogel pattern was deformed to become an inclined cylinder when strong water flow was applied, which proves that it is sticker to one side rather than the other. Our object was focused on the glass slide from both points of view, and from the glass point of view, we could easily see a circle on the left while a crescent grew gradually on the right along the water flow direction as we applied higher pressure to the microfluidic channel. This evidence indicates that PEGDA hydrogel pattern is

easier to be removed from the PDMS side, because the circle shape on the glass side blocked part of the circle that deformed by water pressure on the PDMS side. In addition to that, we disassembled the microfluidic device after photopatterning and looked for the pattern on glass and PDMS separately, and the patterns were found staying on the glass part, which solidified the result above.

As the hydrogel patterns are sticker to the glass rather than PDMS, our priority was to detach the hydrogel from the glass in microfluidic channels. In order to achieve this goal, we proposed to add a sacrificial layer between glass and hydrogel patterns, so that patterns could be debonded from channel walls when the sacrificial layer was dissolved in the presence of a specific chemical treatment. Among numerous water-soluble material candidates, we chose poly(acrylic acid) (PAA) to be the sacrificial layer in our protocol because of the film homogeneity after coating. Furthermore, the water solubility of the PAA layer could be adjusted via ion exchange. Calcium ions can react with carboxylate groups in PAA and produce a water-insoluble PAA-Ca^{2+} layer, and then this polymer could be forced to become water-soluble again with the calcium ions displacement via the addition of excess of sodium ions, shown in Figure 19.[55]

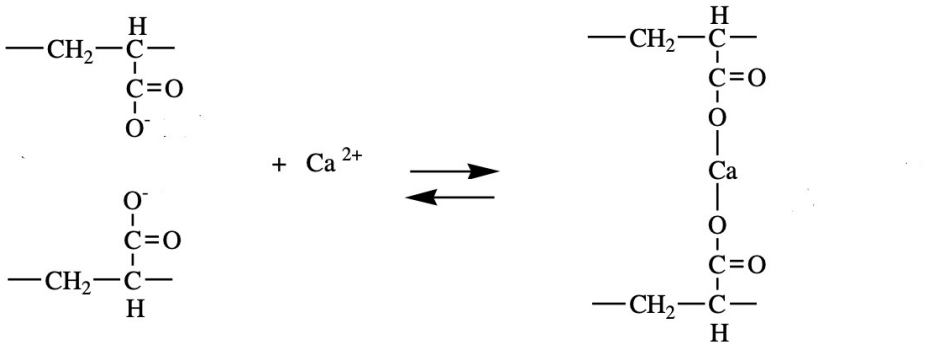

Figure 19. Equation of the reversible ion exchange reaction of calcium ions with the carboxylate groups in poly(acrylic acid) (PAA) polymer.[56]

With the material for the sacrificial layer being determined, firstly we tried flowing 5% w/v PAA solution directly through the microfluidic channel. We expected that a PAA layer would form on the glass side after curing at 150 ºC for 2 minutes, because water takes up the majority of this PAA solution, which would evaporate thoroughly at such a high temperature and the PAA would only occupy the bottom part of the channel. However, it resulted that the 20 μm height channel was so narrow that the PAA layer completely blocked the channel frequently, and the thickness of the PAA layer was hardly uniform, which could potentially affect the resolution of patterning with UV photopolymerization.

Next we tried spin-coating the 5% w/v PAA solution on the entire glass slides with varying velocities to obtain a consistent sacrificial layer at different thicknesses based on the function given by Linder et al.[56] With the PAA layer cured and ion-exchanged on glass surfaces before the assembling of microfluidic devices, there would be a water-insoluble sacrificial layer between the PDMS and the glass slide, and we anticipated a possible leak of the channel because the PAA layer between PDMS and glass would dissolve quickly in the presence of excess sodium ions. The cells spin-coated with DNA leaked much easier than those assembled without any PAA involved according to experiment attempts. In order to prevent the leaks in advance, we tried attaching tape on the margins of the glass slides before spin-coating PAA, so as to make sure that there would be PDMS annealing to the glass directly without any PAA in between and only the center region containing the channel groove would be coated with PAA. Despite its possibility in theory, the protocol did not work properly during actual operations because it was difficult to perfectly match the PDMS channel groove to the sacrificial layer coating region as PAA is colorless and transparent. Besides, it was difficult to control the film thickness of the PAA layer while the tape was applied to the glass during spin-coating, because the tape with height in microns trapped some

of the PAA solution during the rotation of the glass slides and hence the height of PAA sacrificial layer was no longer related to revolution speeds. In addition, in spite of the relative uniformity of PAA layer spin-coated on glass, there was still some UV light scattering through the PAA layer during the photopatterning process, which affected the final resolution of the actual patterns, and this effect could be significant especially for small mask sizes in microns and channels with lower height such as 20 μm.

Then we devised a new microfluidic device preparation method by coating the top PDMS channel with the PAA layer in advance of assembling two PDMS channels together, which is detailed in the method section. This method was inspired by the work of Scneider et al. who designed a microfluidic channel composed of PDMS entirely and then grafted PAA on the channel walls,[57] and the work of Park et al. who combined two half channels for the assembly of a micro-channel.[58] We first tried curing PAA layer in the top channel, and then treated the PAA layer with $CaCl_2$ to turn the layer water insoluble. However, the PAA layer dissolved quickly before we applied photo-curing, and the patterns generated by photopatterning were not able to adhere to the channel walls due to the hydrophobicity of PDMS. As the cured PAA layer was very thick in the microfluidic channel, where only the surface was treated with $CaCl_2$ solution and became water insoluble, the majority of the PAA was still water soluble and dissolved very quickly once water was added in the microfluidic channel. While solution was pushed through microfluidics, the shear force was relatively strong and could break apart the water insoluble surface easily. The entire PAA layer would then dissolve once it was exposed to water molecules.

Then we tried mixing the PAA with $CaCl_2$ solution before curing the PAA layer, and then proceeded with exactly the same curing and photopatterning procedure. The Ca^{2+} crosslinked PAA layer did not dissolve when water was flowed through the channel by pushing relatively hard on 1

mL syringe connected to the channel and it became water soluble after 7 minutes when the 1M NaCl solution flowed through the microfluidic channel, as shown in Figure 20.

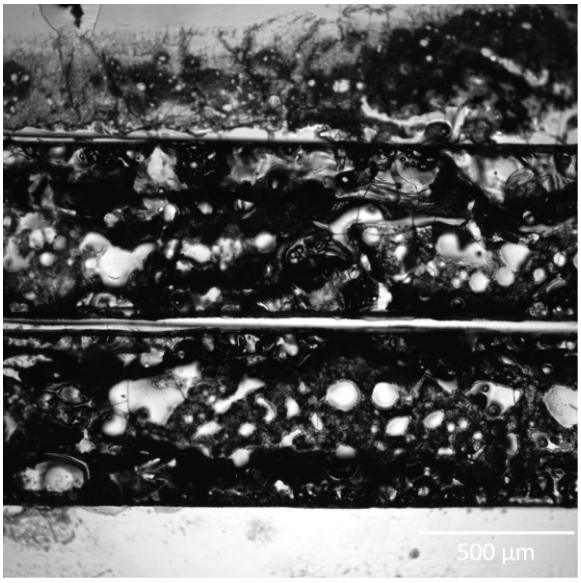

A. Ca^{2+} crosslinked PAA in the microfluidic channel, before any wash

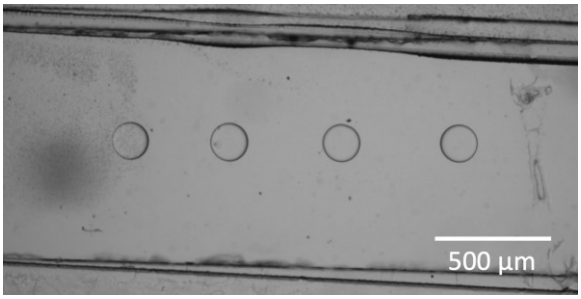

B. After washing with water and photopolymerization with the pregel solution.

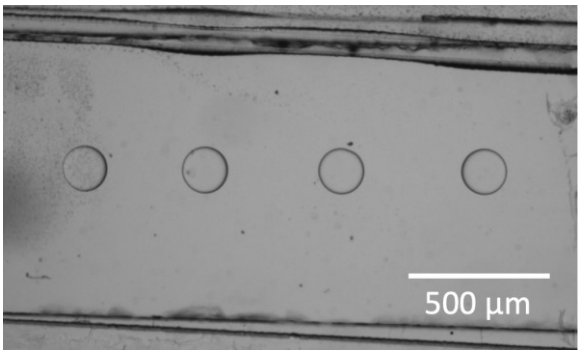

C. After pushing water through a microfluidic channel by hand with relatively strong force.

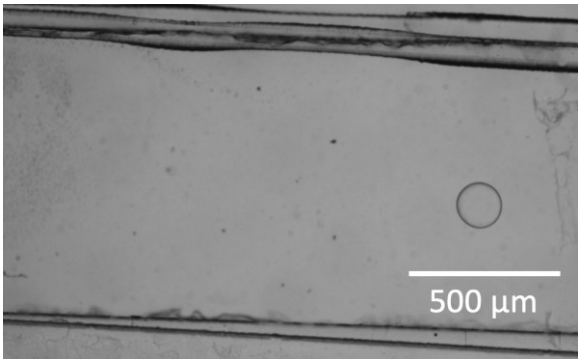

D. 7 minutes after pushing 1M NaCl solution through microfluidic channel.

Figure 20. Step-by-step photo of PEGDA hydrogel patterning and lift-off process in the PAA coated microfluidics channel.

Chapter 3

Conclusion and Future Works

In this work, we applied benzophenone to generate an oxygen quenching region surrounding the microfluidic channel in PDMS to reduce the effects of oxygen inhibition, and photopatterned circular PEGDA hydrogels with a resolution at around 10 μm in diameter. We used a syringe as a microfluidic flow stopper on the channel outlet to balance the pressure inside the microfluidics to achieve stop-flow photolithography during the hydrogel photopatterning process. We also introduced LAP as a water soluble photoinitiator to solve the phase separation problem of pregel solution inside the microfluidic channel. Also, we investigated the effect of UV curing time on hydrogel pattern sizes, and we found a decreasing trend of pattern resolutions with lower photopolymerization time. In addition, we applied PAA as the sacrificial layer coated in microfluidic channel prior to PDMS device assembly, and we used calcium ions (Ca^{2+}) and sodium ions (Na^{+}) to adjust its water solubility for selective release of hydrogel patterns in microfluidic channel.

Further quantitative experiments could be performed for shorter benzophenone diffusion time and more stable hydrogel pattern resolutions. The hydrogel mesh sizes could be investigated for DNA diffusion rates and retention amount in hydrogels with different molecular weights. The entire hydrogel photopatterning in microfluidic channels could be adapted into an automated process controlled by programs and thus more accurate UV exposure time could be achieved to 0.01 seconds. In addition, collection of hydrogels after lift-off from the microfluidic channel could be studied.

Chapter 4

Methods

4.1 PDMS Device Fabrication

4.1.1 Wafer Modification

SU-8 permanent negative photoresist molds for 100 μm and 20 μm height microfluidic cells were built on 4-inch silicon wafers via standard contact photolithography in a clean room. Firstly, wafers were preheated at 200 ºC on a hotplate for 10 minutes to dehydrate the substrate surface, and then different photoresists were applied for mold fabrications with specific heights.

For the manufacturing of 100 μm channel molds, SU-8 3050 (Microchem) was dispensed on the wafer to cover 90% of its surface, and the photoresist was spin coated at 1000 rpm for 30 seconds with the acceleration of 300 rpm/second to obtain a 100 μm film. The wafer was then transferred to a hotplate at 95 ºC for a soft bake for 30 minutes, which is used to inhibit solven evolution. After cooling to room temperature, the photoresist treated side of the wafer was stacked with an AutoCAD designed mask with the channel shapes, and then it was exposed under UV light at a dosage of 225 mJ/cm^2 (i-line). The wafer was transferred to a hotplate at 95 ºC directly after UV exposure for a post-exposure bake for 5 minutes. The wafer was then immersed in SU-8 developer (Microchem) for 15 minutes, and the wafer was rinsed with isopropyl alcohol (IPA) until no white chemical formed. Then the wafer was air dried and baked on a hotplate or in a

convection oven at 200 ºC to further crosslink the material overnight.[59]

The same process was applied during the fabrication of 20 µm height microfluidic molds, except there were some differences on the choice of material and baking time. After dehydrating the substrate, SU-8 10 (Microchem) was used as the photoresist, and a 3000 rpm spin coating for 30 seconds was applied to achieve the film thickness of 10 µm. The wafer was soft baked on a 95 ºC hotplate for 5 minutes, and then the pile of AutoCAD designed mask and the wafer was exposed under UV light at a dosage of 225 mJ/cm^2 (i-line). The 95 ºC post exposure time for 20 µm mold was 2 minutes, and then the wafer was immersed in SU-8 developer (Microchem) for 2 minutes before rinsing with IPA and air drying. Finally the wafer was hard baked at 150 ºC overnight.[60]

4.1.2 PDMS-Glass Microfluidic Device Preparation

Poly-dimethyl-siloxane (PDMS) was made by crosslinking the base elastomer and the curing agent of Sylgard 184 (Dow-Corning) in a 10:1 ratio. Around 50 grams of base elastomer and 5 grams of curing agent would be used for each time, and the two chemicals were well mixed before pouring on the modified wafer according to the previous procedure in a square weighing boat. Then vacuum degassing was applied to the mixture for around 15 minutes to remove most of the air bubbles, and the bubbles existing after vacuum were removed by compressed gas duster (Falcon). After removing all the air bubbles in the mixture above the wafer, the weighing boat was put in a 70 ºC preheated convection oven for an hour to thermally cure the PDMS mold. The PDMS was separated from the wafer by cutting the PDMS surrounding the wafer, and then the PDMS was pulling in the same direction of channel alignment with care. The individual channels were cutted from the PDMS and the channel side was covered by tapes to prevent any impurities. The inlet and outlet of the microfluidic channel were punched with a disposable biopsy punch (Miltex)

in order to obtain a circular hole of 1.5 mm diameter. The customized PDMS was then annealed with a glass coverslip (Fisher Scientific) via oxygen plasma. Glass slides and PDMS channels were put in the chamber of the planar etcher (Technics) with the channels on top, and then the lid was closed. Vacuum degassing was used before the chamber was refilled with oxygen to a pressure of 0.3-0.5 Torr. Then the oxygen plasma was applied at around 45 watts for approximately 40 seconds. After venting the chamber, the PDMS was attached directly to the glass and then put on a hotplate or in an oven preheated at 80 ºC for at least 2 hours for further annealing.

4.2 Photopatterning 10% PEGDA Hydrogel with benzophenone treatment

4.2.1 With Omnirad 2100 photoinitiator

Benzophenone was used to pretreat the device before the addition of pregel solution. Benzophenone power was dissolved in ethanol to make a 10% w/v solution, and the solution was mixed well before being loaded to the microfluidic channel with a syringe. The microfluidic device was put in the dark for 30 minutes to prevent any possible benzophenone photoinitiation. Omnirad 2100 was diluted in butanol to obtain a 75% photoinitiator stock. The pregel solution was prepared in a total volume of 1 mL according to the protocol shown in Table A below.

Material	**MilliQ H_2O**	**10X TAE**	**PEGDA 575**	**75% Omnirad in butanol**	**Total**
Volume (µL)	760	100	100	40	1000
Final Solution		1X TAE	10% PEGDA 575	3% Omnirad	

Table A1. Recipe of 10% PEGDA 575 pregel solution with Omnirad 2100 as photoinitiator.

After vortexing to thoroughly mix the pregel solution (for approximately 30 seconds), the tube was then centrifuged for another 30 seconds to accelerate the precipitation of excess photoinitiator. 300-500 μL supernatant of the pregel solution was taken and was loaded into microfluidic channels with syringe or syringe with tubing. Phase consistency of liquid was checked inside the channel, more pregel solution was loaded if there was air or any inconsistent phase.

A digital light projection device containing a Mightex System Polygon 400 Dense Pixel micromirror array was used for the photopolymerization process. An inverted Olympus IX73 microscope was used for light focusing and objective locating, and a digital camera (HAMAMATSU) was applied for the recording of experiment results. Blue light emitting from LED was reflected by the digital micromirror array selectively according to the AutoCAD designed digital mask, and then a pattern could show at the desired place by adjusting the multi-axis stage controller (ASI) and the microscope objective.

After the microfluidic device was fixed on the XY automated microscope stage (ASI) located on a focusing translation platform (ASI), the channel was focused via a LMU-20X-Nuv microscope objective. Polyscan2 was used as the interface to control shape and intensity of blue light, and then the light source was converted to 365 nm UV light (Mightex). UV exposure was applied specifically to the focused location for 1-5 seconds, where patterns would form gradually during this time.

4.2.2 With Lithium phenyl -2,4,6- trimethylbenzoyl-phosphinate (LAP) Photoinitiator

The method of photopatterning 10% PEGDA hydrogel with LAP as photoinitiator is the same as that with Omnirad 2100, except a little difference in the protocol of pregel solution

preparation, shown in Table B. Besides, there would be no problem of phase separation as LAP has good water solubility, so it was unnecessary to centrifuge the pregel solution after well mixing.

Material	MilliQ H_2O	10X TAE	PEGDA 575	1 wt% LAP in MilliQ H_2O	Total
Volume (µL)	700	100	100	100	1000
Final Solution		1X TAE	10% PEGDA 575	0.1 wt%	

Table A2. Recipe of 10% PEGDA 575 pregel solution with LAP as photoinitiator.

4.3 Release of Patterns from the Microfluidic Channel by Applying a Polyacrylic Acid (PAA) Sacrificial Layer

4.3.1 PAA-$CaCl_2$ Solution Preparation

Solid $CaCl_2$ was dissolved in MilliQ water to make 1 mL of 5 M $CaCl_2$ stock solution. PAA was purchased as 25% stock with the average molecular weight of around 50,000 from Polyscience. Then the 5 mL of 5% PAA solution was prepared according to the recipe shown in Table C, and the solution was vortexed until it became well mixed.

Material	MilliQ H_2O	25% PAA	5 M $CaCl_2$	Total
Volume (mL)	3	1	1	5
Final Solution		5% PAA	1M $CaCl_2$	

Table A3. Recipe of PAA-$CaCl_2$ solution preparation.

4.3.2 PAA Microfluidic Device Fabrication

Instead of the PDMS-Glass microfluidic devices assembled with the methods in the above section, we adjusted the previous procedure and devised an approach of fabricating microfluidic channels enclosed by PDMS only. PDMS channels were prepared in the same procedure as those in PDMS glass device preparation. After the PDMS channels were separated from the silicon wafer and cutted into individual pieces, we added the PAA-$CaCl_2$ solution prepared in the previous step to half of the PDMS channels. Then the extra PAA-$CaCl_2$ solution left on the PDMS surface was erased with a blade, trapping the solution in the channel groove. The purpose of this step was to prevent the PDMS microfluidic device from leaking due to the dissolving of the PAA layer, and this action was also used to remove the ridge of PAA-$CaCl_2$ solution because of surface tension to obtain a relatively flat liquid surface. The PDMS channel was then put in a convection oven preheated to 150 ºC with the channel groove on top to thermally cure the PAA for 30 minutes. Then we punched circular holes with a diameter of 1.5 mm at the inlets and outlets off all PDMS microfluidic channels. After hole punching, all PDMS channels were treated with O_2 plasma (Technics) for better annealing ability. We took a PAA treated PDMS channel and another untreated PDMS, and matched their holes at the inlet and outlet on both parts to confirm the alignment of two channel grooves, before attaching the two PDMS pieces. Then we took the assembled PDMS channel and applied O_2 plasma on the side that was not coated with PDMS together with a glass slide (Fisher Scientific). The aim of this step was to block the bottom opening of holes at the inlet and outlet of the PDMS channel to prevent solution flowing out of the tunnels directly from the bottom. After the PDMS channel was attached to the glass slide, we further annealed the microfluidic device in an 80 ºC oven for 2 hours.

4.3.3 Photopolymerization of PEGDA Hydrogel and Release Process

The channel was rinsed with water by hand for approximately 30 seconds to wash out extra $CaCl_2$ until the channel appeared clean and transparent under the microscope. The pregel solution was prepared with the same recipe as Table A or Table B depending on the choice of photoinitiator. Then the patterning procedure was conducted with the same process as that in the previous protocol. Specific masks were used with 20X Nuv microscope objectives to obtain the desired pattern shape. After patterns were successfully generated, water flowed through the channel by hand with relatively strong force to rinse out the pregel solution. For release of hydrogel patterns from microfluidic channels, 1M NaCl solution in water was required to rinse the channel for around 7 minutes before pattern movement.

5 Bibliography

(1) Ben-Ari, M.; Mondada, F. Robots and Their Applications. In *Elements of Robotics*; Ben-Ari, M., Mondada, F., Eds.; Springer International Publishing: Cham, 2018; pp 1–20. https://doi.org/10.1007/978-3-319-62533-1_1.

(2) Banerjee, H.; Suhail, M.; Ren, H. Hydrogel Actuators and Sensors for Biomedical Soft Robots: Brief Overview with Impending Challenges. *Biomimetics* **2018**, *3* (3), 15. https://doi.org/10.3390/biomimetics3030015.

(3) Soto, F.; Wang, J.; Ahmed, R.; Demirci, U. Medical Micro/Nanorobots in Precision Medicine. *Adv. Sci.* **2020**, *7* (21), 2002203. https://doi.org/10.1002/advs.202002203.

(4) Kim, D.-I.; Lee, H.; Kwon, S.-H.; Sung, Y. J.; Song, W. K.; Park, S. Bilayer Hydrogel Sheet-Type Intraocular Microrobot for Drug Delivery and Magnetic Nanoparticles Retrieval. *Adv. Healthc. Mater.* **2020**, *9* (13), 2000118. https://doi.org/10.1002/adhm.202000118.

(5) Hu, W.; S. Ishii, K.; Fan, Q.; T. Ohta, A. Hydrogel Microrobots Actuated by Optically Generated Vapour Bubbles. *Lab. Chip* **2012**, *12* (19), 3821–3826. https://doi.org/10.1039/C2LC40483D.

(6) Jeon, S.; Kim, S.; Ha, S.; Lee, S.; Kim, E.; Kim, S. Y.; Park, S. H.; Jeon, J. H.; Kim, S. W.; Moon, C.; Nelson, B. J.; Kim, J.; Yu, S.-W.; Choi, H. Magnetically Actuated Microrobots as a Platform for Stem Cell Transplantation. *Sci. Robot.* **2019**, *4* (30). https://doi.org/10.1126/scirobotics.aav4317.

(7) Chen, S.; Cao, Y.; Sarparast, M.; Yuan, H.; Dong, L.; Tan, X.; Cao, C. Soft Crawling Robots: Design, Actuation, and Locomotion. *Adv. Mater. Technol.* **2020**, *5* (2), 1900837. https://doi.org/10.1002/admt.201900837.

(8) Xie, M.; Zhang, W.; Fan, C.; Wu, C.; Feng, Q.; Wu, J.; Li, Y.; Gao, R.; Li, Z.; Wang, Q.; Cheng, Y.; He, B. Bioinspired Soft Microrobots with Precise Magneto-Collective Control for Microvascular Thrombolysis. *Adv. Mater.* **2020**, *32* (26), 2000366. https://doi.org/10.1002/adma.202000366.

(9) Kim, S.; Laschi, C.; Trimmer, B. Soft Robotics: A Bioinspired Evolution in Robotics. *Trends Biotechnol.* **2013**, *31* (5), 287–294. https://doi.org/10.1016/j.tibtech.2013.03.002.

(10) Rus, D.; Tolley, M. T. Design, Fabrication and Control of Soft Robots. *Nature* **2015**, *521* (7553), 467–475. https://doi.org/10.1038/nature14543.

(11) Li, D.; Liu, C.; Yang, Y.; Wang, L.; Shen, Y. Micro-Rocket Robot with All-Optic Actuating and Tracking in Blood. *Light Sci. Appl.* **2020**, *9* (1), 84. https://doi.org/10.1038/s41377-020-0323-y.

(12) Park, S. J.; Park, S.-H.; Cho, S.; Kim, D.-M.; Lee, Y.; Ko, S. Y.; Hong, Y.; Choy, H. E.; Min, J.-J.; Park, J.-O.; Park, S. New Paradigm for Tumor Theranostic Methodology Using Bacteria-Based Microrobot. *Sci. Rep.* **2013**, *3* (1), 3394. https://doi.org/10.1038/srep03394.

(13) Tasoglu, S.; Diller, E.; Guven, S.; Sitti, M.; Demirci, U. Untethered Micro-Robotic Coding of Three-Dimensional Material Composition. *Nat. Commun.* **2014**, *5* (1), 3124. https://doi.org/10.1038/ncomms4124.

(14) Raza, A.; Rasheed, T.; Nabeel, F.; Hayat, U.; Bilal, M.; Iqbal, H. M. N. Endogenous and Exogenous Stimuli-Responsive Drug Delivery Systems for Programmed Site-Specific Release. *Molecules* **2019**, *24* (6). https://doi.org/10.3390/molecules24061117.

(15) Werner, S. L.; Barken, D.; Hoffmann, A. Stimulus Specificity of Gene Expression Programs Determined by Temporal Control of IKK Activity. *Science* **2005**, *309* (5742), 1857–1861. https://doi.org/10.1126/science.1113319.

(16) Cangialosi, A.; Yoon, C.; Liu, J.; Huang, Q.; Guo, J.; Nguyen, T. D.; Gracias, D. H.; Schulman, R. DNA Sequence–Directed Shape Change of Photopatterned Hydrogels via High-Degree Swelling. *Science* **2017**, *357* (6356), 1126–1130. https://doi.org/10.1126/science.aan3925.

(17) Lee, Y.; Song, W. J.; Sun, J.-Y. Hydrogel Soft Robotics. *Mater. Today Phys.* **2020**, *15*, 100258. https://doi.org/10.1016/j.mtphys.2020.100258.

(18) Moran, C.; Levingstone, T. Biofunctional Materials for Bone and Cartilage Tissue Engineering. In *Reference Module in Materials Science and Materials Engineering*; Elsevier, 2020. https://doi.org/10.1016/B978-0-12-803581-8.11791-6.
(19) Peppas, N. A.; Slaughter, B. V.; Kanzelberger, M. A. 9.20 - Hydrogels. In *Polymer Science: A Comprehensive Reference*; Matyjaszewski, K., Möller, M., Eds.; Elsevier: Amsterdam, 2012; pp 385–395. https://doi.org/10.1016/B978-0-444-53349-4.00226-0.
(20) Lin, C.-C.; Anseth, K. S. PEG Hydrogels for the Controlled Release of Biomolecules in Regenerative Medicine. *Pharm. Res.* **2009**, *26* (3), 631–643. https://doi.org/10.1007/s11095-008-9801-2.
(21) Hutanu, D. Recent Applications of Polyethylene Glycols (PEGs) and PEG Derivatives. *Mod. Chem. Appl.* **2014**, *02* (02). https://doi.org/10.4172/2329-6798.1000132.
(22) Zarrintaj, P.; Saeb, M. R.; Jafari, S. H.; Mozafari, M. Chapter 18 - Application of Compatibilized Polymer Blends in Biomedical Fields. In *Compatibilization of Polymer Blends*; A.r., A., Thomas, S., Eds.; Elsevier, 2020; pp 511–537. https://doi.org/10.1016/B978-0-12-816006-0.00018-9.
(23) Kotturi, H.; Abuabed, A.; Zafar, H.; Sawyer, E.; Pallipparambil, B.; Jamadagni, H.; Khandaker, M. Evaluation of Polyethylene Glycol Diacrylate-Polycaprolactone Scaffolds for Tissue Engineering Applications. *J. Funct. Biomater.* **2017**, *8* (3). https://doi.org/10.3390/jfb8030039.
(24) Yang, W.; Yu, H.; Wang, Y.; Liu, L. Hydrogel Printing Based on UV-Induced Projection for Cell-Based Microarray Fabrication. In *Cell-Based Microarrays: Methods and Protocols*; Ertl, P., Rothbauer, M., Eds.; Methods in Molecular Biology; Springer: New York, NY, 2018; pp 97–105. https://doi.org/10.1007/978-1-4939-7792-5_8.
(25) Wang, W.; Narain, R.; Zeng, H. Chapter 10 - Hydrogels. In *Polymer Science and Nanotechnology*; Narain, R., Ed.; Elsevier, 2020; pp 203–244. https://doi.org/10.1016/B978-0-12-816806-6.00010-8.
(26) Zhu, J.; Hu, J.; Marchant, R. E. 9 - Biomimetic Hydrogels as Scaffolds for Tissue-Engineering Applications. In *Biomimetic Biomaterials*; Ruys, A. J., Ed.; Woodhead Publishing Series in Biomaterials; Woodhead Publishing, 2013; pp 238–275. https://doi.org/10.1533/9780857098887.2.238.
(27) Huh, J. T.; Yoo, J. J.; Atala, A.; Lee, S. J. Chapter 74 - Three-Dimensional Bioprinting for Tissue Engineering. In *Principles of Tissue Engineering (Fifth Edition)*; Lanza, R., Langer, R., Vacanti, J. P., Atala, A., Eds.; Academic Press, 2020; pp 1391–1415. https://doi.org/10.1016/B978-0-12-818422-6.00076-9.
(28) Berry, D. B.; Yu, C.; Chen, S. Chapter 75 - Biofabricated Three-Dimensional Tissue Models. In *Principles of Tissue Engineering (Fifth Edition)*; Lanza, R., Langer, R., Vacanti, J. P., Atala, A., Eds.; Academic Press, 2020; pp 1417–1441. https://doi.org/10.1016/B978-0-12-818422-6.00077-0.
(29) Dikshit, V.; Goh, G. D.; Nagalingam, A. P.; Goh, G. L.; Yeong, W. Y. Chapter 17 - Recent Progress in 3D Printing of Fiber-Reinforced Composite and Nanocomposites. In *Fiber-Reinforced Nanocomposites: Fundamentals and Applications*; Han, B., Sharma, S., Nguyen, T. A., Longbiao, L., Bhat, K. S., Eds.; Micro and Nano Technologies; Elsevier, 2020; pp 371–394. https://doi.org/10.1016/B978-0-12-819904-6.00017-7.
(30) Yang, W.; Cai, S.; Chen, Y.; Liang, W.; Lai, Y.; Yu, H.; Wang, Y.; Liu, L. Modular and Customized Fabrication of 3D Functional Microgels for Bottom-Up Tissue Engineering and Drug Screening. *Adv. Mater. Technol.* **2020**, *5* (5), 1900847. https://doi.org/10.1002/admt.201900847.
(31) Fallahi, H.; Zhang, J.; Phan, H.-P.; Nguyen, N.-T. Flexible Microfluidics: Fundamentals, Recent Developments, and Applications. *Micromachines* **2019**, *10* (12). https://doi.org/10.3390/mi10120830.
(32) Tentori, A. M.; Herr, A. E. Photopatterned Materials in Bioanalytical Microfluidic Technology. *J. Micromechanics Microengineering Struct. Devices Syst.* **2011**, *21* (5), 054001. https://doi.org/10.1088/0960-1317/21/5/054001.
(33) Cheung, P.; Toda-Peters, K.; Shen, A. Q. In Situ Pressure Measurement within Deformable Rectangular Polydimethylsiloxane Microfluidic Devices. *Biomicrofluidics* **2012**, *6* (2), 026501. https://doi.org/10.1063/1.4720394.

(34) Wu, M.-H.; Paul, K. E.; Whitesides, G. M. Patterning Flood Illumination with Microlens Arrays. *Appl. Opt.* **2002**, *41* (13), 2575–2585. https://doi.org/10.1364/AO.41.002575.
(35) Yang, Y.; Leong, K. W. Chapter 3 - Microfluidic Platforms with Nanoscale Features. In *Microfluidic Cell Culture Systems (Second Edition)*; Borenstein, J. T., Tandon, V., Tao, S. L., Charest, J. L., Eds.; Micro and Nano Technologies; Elsevier, 2019; pp 65–90. https://doi.org/10.1016/B978-0-12-813671-3.00003-7.
(36) Merkel, T. C.; Bondar, V. I.; Nagai, K.; Freeman, B. D.; Pinnau, I. Gas Sorption, Diffusion, and Permeation in Poly(Dimethylsiloxane). *J. Polym. Sci. Part B Polym. Phys.* **2000**, *38* (3), 415–434. https://doi.org/10.1002/(SICI)1099-0488(20000201)38:3<415::AID-POLB8>3.0.CO;2-Z.
(37) Annabestani, M.; Esmaeili-Dokht, P.; Fardmanesh, M. A Novel, Low Cost, and Accessible Method for Rapid Fabrication of the Modifiable Microfluidic Devices. *Sci. Rep.* **2020**, *10* (1), 16513. https://doi.org/10.1038/s41598-020-73535-w.
(38) Dendukuri, D.; Pregibon, D. C.; Collins, J.; Hatton, T. A.; Doyle, P. S. Continuous-Flow Lithography for High-Throughput Microparticle Synthesis. *Nat. Mater.* **2006**, *5* (5), 365–369. https://doi.org/10.1038/nmat1617.
(39) Dendukuri, D.; Gu, S. S.; Pregibon, D. C.; Hatton, T. A.; Doyle, P. S. Stop-Flow Lithography in a Microfluidic Device. *Lab. Chip* **2007**, *7* (7), 818–828. https://doi.org/10.1039/B703457A.
(40) Solute Diffusion within Hydrogels. Mechanisms and Models | Macromolecules https://pubs.acs.org/doi/10.1021/ma980765f (accessed Feb 19, 2021).
(41) Ligon, S. C.; Husár, B.; Wutzel, H.; Holman, R.; Liska, R. Strategies to Reduce Oxygen Inhibition in Photoinduced Polymerization. *Chem. Rev.* **2014**, *114* (1), 557–589. https://doi.org/10.1021/cr3005197.
(42) Alvankarian, J.; Majlis, B. Y. Exploiting the Oxygen Inhibitory Effect on UV Curing in Microfabrication: A Modified Lithography Technique. *PLoS ONE* **2015**, *10* (3). https://doi.org/10.1371/journal.pone.0119658.
(43) Studer, K.; Decker, C.; Beck, E.; Schwalm, R. Overcoming Oxygen Inhibition in UV-Curing of Acrylate Coatings by Carbon Dioxide Inerting, Part I. *Prog. Org. Coat.* **2003**, *48* (1), 92–100. https://doi.org/10.1016/S0300-9440(03)00120-6.
(44) Bolon, D. A.; Webb, K. K. Barrier Coats versus Inert Atmospheres. The Elimination of Oxygen Inhibition in Free-Radical Polymerizations. *J. Appl. Polym. Sci.* **1978**, *22* (9), 2543–2551. https://doi.org/10.1002/app.1978.070220913.
(45) Oytun, F.; Kahveci, M. U.; Yagci, Y. Sugar Overcomes Oxygen Inhibition in Photoinitiated Free Radical Polymerization. *J. Polym. Sci. Part Polym. Chem.* **2013**, *51* (8), 1685–1689. https://doi.org/10.1002/pola.26554.
(46) Bühler, J.; Steiner, F.-P.; Baltes, H. Silicon Dioxide Sacrificial Layer Etching in Surface Micromachining. *J. Micromechanics Microengineering* **1997**, *7* (1), R1–R13. https://doi.org/10.1088/0960-1317/7/1/001.
(47) Olanrewaju, A.; Beaugrand, M.; Yafia, M.; Juncker, D. Capillary Microfluidics in Microchannels: From Microfluidic Networks to Capillaric Circuits. *Lab. Chip* **2018**, *18* (16), 2323–2347. https://doi.org/10.1039/C8LC00458G.
(48) Sung, J.; Lee, D. G.; Lee, S.; Park, J.; Jung, H. W. Crosslinking Dynamics and Gelation Characteristics of Photo- and Thermally Polymerized Poly(Ethylene Glycol) Hydrogels. *Materials* **2020**, *13* (15). https://doi.org/10.3390/ma13153277.
(49) Dorsey, P. J.; Rubanov, M.; Wang, W.; Schulman, R. Digital Maskless Photolithographic Patterning of DNA-Functionalized Poly(Ethylene Glycol) Diacrylate Hydrogels with Visible Light Enabling Photodirected Release of Oligonucleotides. *ACS Macro Lett.* **2019**, *8* (9), 1133–1140. https://doi.org/10.1021/acsmacrolett.9b00450.
(50) Yuk, H.; Zhang, T.; Parada, G. A.; Liu, X.; Zhao, X. Skin-Inspired Hydrogel–Elastomer Hybrids with Robust Interfaces and Functional Microstructures. *Nat. Commun.* **2016**, *7* (1), 12028. https://doi.org/10.1038/ncomms12028.
(51) Humans, I. W. G. on the E. of C. R. to. *BENZOPHENONE*; International Agency for Research on

Cancer, 2013.
(52) Schneider, M. H.; Tran, Y.; Tabeling, P. Benzophenone Absorption and Diffusion in Poly(Dimethylsiloxane) and Its Role in Graft Photo-Polymerization for Surface Modification. *Langmuir* **2011**, *27* (3), 1232–1240. https://doi.org/10.1021/la103345k.
(53) Tatti, F.; Papini, M. P.; Raboni, M.; Viotti, P. Image Analysis Procedure for Studying Back-Diffusion Phenomena from Low-Permeability Layers in Laboratory Tests. *Sci. Rep.* **2016**, *6* (1), 30400. https://doi.org/10.1038/srep30400.
(54) Fairbanks, B. D.; Schwartz, M. P.; Bowman, C. N.; Anseth, K. S. Photoinitiated Polymerization of PEG-Diacrylate with Lithium Phenyl-2,4,6-Trimethylbenzoylphosphinate: Polymerization Rate and Cytocompatibility. *Biomaterials* **2009**, *30* (35), 6702–6707. https://doi.org/10.1016/j.biomaterials.2009.08.055.
(55) Schweins, R.; Huber, K. Collapse of Sodium Polyacrylate Chains in Calcium Salt Solutions. *Eur. Phys. J. E* **2001**, *5* (1), 117–126. https://doi.org/10.1007/s101890170093.
(56) Linder, V.; Gates, B. D.; Ryan, D.; Parviz, B. A.; Whitesides, G. M. Water-Soluble Sacrificial Layers for Surface Micromachining. *Small* **2005**, *1* (7), 730–736. https://doi.org/10.1002/smll.200400159.
(57) Schneider, M. H.; Willaime, H.; Tran, Y.; Rezgui, F.; Tabeling, P. Wettability Patterning by UV-Initiated Graft Polymerization of Poly(Acrylic Acid) in Closed Microfluidic Systems of Complex Geometry. *Anal. Chem.* **2010**, *82* (21), 8848–8855. https://doi.org/10.1021/ac101345m.
(58) Park, S. E.; Georgescu, A.; Huh, D. Organoids-on-a-Chip. *Science* **2019**, *364* (6444), 960–965. https://doi.org/10.1126/science.aaw7894.
(59) SU-8 3000 for Microstructure Fabrication | Kayaku Advanced Materials. *Kayaku Advanced Materials, Inc.*
(60) SU-8. *Kayaku Advanced Materials, Inc.*

6 CV

Zhe Chen

3700 N. Charlest Street, Baltimore, MD 21218 | (949) 537-9577 | zchen83@jhu.edu

---

EDUCATION

Johns Hopkins University, Baltimore, MD GPA:3.63

Master of Science in Chemical Engineering Expected May 2021

Relevant Courses: Thermodynamics, Statistical mechanics, Kinetics, Metabolic System Biotechnology, Interfacial Science with Application to Nanoscale Systems, Introduction to Polymeric Materials, Transport Phenomena

University of California, Irvine, Irvine, CA GPA: 3.25

Bachelor of Science in Chemical Engineering June 2019

Bachelor of Science in Chemistry June 2019

PROFESSIONAL EXPERIENCE

Graduate Student in Schulman Lab, **Multi-domain DNA-crosslinked Hydrogel Automated Digital Patterning** Oct 2019 - Present

- Controlled digital micromirror device (DMD) for hydrogel photopatterning, including preparation of PDMS devices, silicon mold, use of 20X Microscope, and related software.
- Limited oxygen inhibition during photopatterning by applying oxygen diffusion barrier and oxygen scavenger.
- Identified factors that influence reliable hydrogel photopolymerization in 20 μm devices.
- Applied sacrificial layers for hydrogel pattern lift-off in microfluidic channels.

Intern, **Technical Development Department, Jiangsu Sobute Ltd.** July 2018

- Looked for the new-type polycarboxylate superplasticizer with phosphoric acid functional groups.
- Tested the usability of polycarboxylate superplasticizer.
- Looked for related literature, constructed the molecular modules, made new-type superplasticizer, and studied its nature.

Intern, **Marketing and Technical Service Department, BASF SE** August 2018

- On-site experiments and practical operations for the customers.
- Understood the industry changes, market dynamics, the needs of the customers for certain products.

Projects, **University of California, Irvine**

September 2017 – June 2019

- *Team Leader,* **Free and Forced Convection**
- *Member in Charge of Results and Calculation,* **The Study of the Process of Aeration**
- *Member in Charge of Calculation and Discussion,* **The Study on Material Transfer during the Process of Activated Carbon Adsorption**
- *Member in Charge of Introduction,* **The Study on Nano Photocatalyst**
- *Member in Charge of Results and Calculation,* **Tray Dryer**

TECHNICAL SKILLS

Computer programming: Python, MATLAB, Simulink, Mathematica, C, Office Set (Excel, Word), Spartan Student, Logger Pro, pyMOL, ChemDraw

Lab appliances: Microscope, LabQuest, VISNIR Spectrometer, IR spectrum, NMR spectrum, Alpha and Neutron survey meter, Geiger-Mueller detector, HPGe detector, LaBert3 detector

Languages: English and Chinese